ADVANCED OPTICAL MATERIALS
www.advopticalmat.de

Selectively Tunable Luminescence of Perovskite Nanocrystals Embedded in Polymer Matrix Allows Direct Laser Patterning

Chantal Martin, Anatol Prudnikau, Leonardo Orazi, Nikolai Gaponik, and Vladimir Lesnyak**

Cesium lead halide perovskite nanocrystals (NCs) have gained enormous attention as promising light-emitting and light-converting materials. Most of their applications require embedding NCs in various matrices, which is a challenging task due to their low stability, especially in the case of red-emitting $CsPbI_3$ NCs. In this work, a new approach is proposed allowing the formation of red-emitting perovskite NCs by anion exchange induced directly inside a solid polymer matrix using green-emitting $CsPbBr_3$ NCs as templates and iodododecane as an iodine source. Moreover, a simple and efficient route to photo-assisted termination of the anion exchange reaction in the polymer composite after reaching desired optical properties is demonstrated. The findings allow the authors to pattern a thin composite film with an ultrashort UV laser resulting in a selective generation of green- and red-emitting features with a 15 µm resolution.

1. Introduction

In recent years, all-inorganic cesium lead halide perovskite $CsPbX_3$ (X = Cl^-, Br^-, or I^-) nanocrystals (NCs) have attracted tremendous scientific and technological interest as promising materials for light-emitting technologies due to their outstanding optical properties.[1–3] These NCs exhibit a high absorption coefficient, narrow photoluminescence (PL) bandwidth, and high defect tolerance that result in near unity PL quantum yields (QYs).[4–6] The emission wavelength of $CsPbX_3$ NCs can be precisely tuned across almost the entire visible range (400–700 nm) by simply tailoring their halide composition.[7,8] To date, a range of reliable synthetic methods for a precise control of size, shape, and composition of colloidal perovskite NCs have been developed.[9] Liquid-phase methods, such as hot-injection and ligand-assisted reprecipitation, are the most-developed synthetic approaches. The hot-injection method is based on a fast injection of one precursor into a hot solution of the second in a high boiling solvent, where ligands provide colloidal stability of the growing NCs.[8,10] This method enables producing small-sized NCs with a narrow size distribution[11] but requires an inert atmosphere and is poorly scalable. The ligand-assisted precipitation method is based on addition of a nonpolar solvent (such as hexane or toluene) containing ligands into a polar solvent such as dimethylformamide or dimethyl sulfoxide containing precursor salts. This leads to an oversaturation of the precursors and their spontaneous crystallization even at room temperature (RT).[12,13] This method does not require specific equipment and can easily be scaled up. The disadvantage of this method is a difficulty in separating the nucleation and growth stages resulting in a relatively broad size distribution.[9]

In addition to direct synthetic approaches, the composition and thus optical properties of perovskite NCs can be changed in a post-synthetic treatment through an ion exchange process.[14] Kovalenko's and Manna's groups were first to report instant and reversible anion exchange after adding various halogen sources (such as Grignard reagents or oleylammonium halides) to a colloidal solution of $CsPbX_3$ NCs.[15,16] The chemical bonding in $CsPbX_3$ NCs is much more ionic than, for example, the highly covalent lattices of metal chalcogenides, which leads to a low formation energy of the perovskite NCs and as a result to easier postsynthetic transformation.[17] In addition, the high intrinsic concentration of halide vacancies results in increased mobility of the halide ions,[18] that, in turn, facilitates the anion transfer and exchange processes.[16,19]

On the one hand, high ionicity and low crystal lattice energy allowed the facile synthesis and postsynthetic transformations of the NCs. On the other hand, the same factors are responsible for the low stability against polar solvents, humidity, oxygen, light, and elevated temperatures.[20] Even at RT, $CsPbX_3$

C. Martin, A. Prudnikau, N. Gaponik, V. Lesnyak
Physical Chemistry
TU Dresden
Zellescher Weg 19, 01069 Dresden, Germany
E-mail: nikolai.gaponik@tu-dresden.de;
vladimir.lesnyak1@tu-dresden.de
L. Orazi
Department of Sciences and Methods for Engineering
University of Modena and Reggio
Via Amendola 2, Emilia, Reggio Emilia 42122, Italy

The ORCID identification number(s) for the author(s) of this article can be found under https://doi.org/10.1002/adom.202200201.

DOI: 10.1002/adom.202200201

NCs can quickly transform into a more stable nonperovskite orthorhombic phase, resulting in a complete change in their initial optical properties.[9] Different approaches were developed to improve structural and environmental stability of perovskite NCs. They include surface engineering,[21–23] doping,[24,25] and matrix encapsulation. The latter can be performed by incorporating the NCs in various robust inorganic matrices, such as salts,[26] silica,[27] glass,[28,29] and zeolite,[30] or in polymers. The encapsulation of perovskite NCs in polymer matrices provides the advantage of efficient protection in combination with the processability of the NCs and polymer solutions by drop-casting, spray- and spin-coating, and other film-forming technologies promising for optical applications.[31–33] Furthermore, polymer matrices are attractive due to their low cost, accessibility at an industrial scale, and an opportunity of chemical modifications. Superior optical properties and enhanced stability make light-emitting perovskite NCs-in-polymer composites a material of choice for down-conversion applications in displays and solid state lighting.[34]

Different routes have been applied for preparing polymer composites with embedded $CsPbX_3$ NCs. The most straightforward approach involves blending of colloidal $CsPbX_3$ NCs and a polymer in a common solvent and forming polymer composites after the solvent evaporation.[35] The second approach is the chemical anchoring of polymers onto the NC surface, which minimizes phase separation in the composite due to strong interactions between embedded nanoparticles and the matrix.[36] Of particular interest is the in situ synthesis of perovskite-polymer composites by mixing precursors with polymers and forming NCs directly in the polymer matrix.[37] This approach avoids damaging of low-stable perovskite NCs during isolation from the reaction system, purification, and transfer into a polymer matrix. This issue is especially relevant for $CsPbI_3$ NCs because their Goldschmidt tolerance factor is near 0.8, which is very close to the edge of the range of the stability requirements for 3D perovskite structures (0.76–1.13).[9,38] The in situ synthesis of fluorescent semiconductor NCs can benefit the development of manufacturing methods directly applicable to produce optoelectronic devices.[39]

In this work, we report in situ Br^--to-I^- anion exchange in $CsPbBr_3$ NCs directly in well protecting and processable polymer matrices using iodododecane (IDD) as an iodine source that allows precise tuning of the PL of the final composites in the spectral range of 520–680 nm. We have analyzed the structure, morphology, and optical properties of perovskite NCs obtained by anion exchange in polymer films. In addition, we propose a simple and powerful tool for photochemical termination of the anion exchange in the polymer composite after reaching the desired PL color. Direct patterning of luminescent pixels with a resolution of about 15 µm was demonstrated by applying a picosecond UV laser. This method opens up great opportunities in flexible production of small- and mid-size batches of display devices.

2. Results and Discussion

The strategy used in this work to obtain green and red luminescing composite films with embedded $CsPbX_3$ NCs is schematically shown in **Figure 1**. Green-emitting $CsPbBr_3$ NCs of 9.3 nm in size (**Figure 2** and Figure S1a, Supporting Information) with narrow PL centered at 514 nm and PLQY of 90% were synthesized, as described by the Manna group[10] with some minor modifications (see details in the Experimental Section).

The as-synthesized NCs capped with long-chain organic molecules (oleic acid and oleylamine) were mixed with a solution of poly(methyl methacrylate-*co*-lauryl methacrylate) [(P(MMA-*co*-LMA)] in toluene. The resulting mixture was used to prepare composite films on glass substrates via drop-casting. Lauryl chains of P(MMA-*co*-LMA) can interact with long-chain molecules on the NC surface, preventing them from aggregation after the solvent evaporation and providing their homogenous distribution in the polymer matrix. As can be seen from the photographs in Figure 2c, the resulting composite films with the thickness of ≈50 µm are transparent and show no signs of a phase separation. For the Br^--to-I^- exchange in perovskite NCs embedded in polymer films, IDD, as a source of iodine, was introduced into the system in various molar ratios relative to the amount of $CsPbBr_3$. Both the polymer used for the film preparation and IDD have the same hydrocarbon chains, which ensure excellent compatibility between the matrix and the precursor and lead to a homogeneous distribution of IDD in the films. This homogeneity is important to achieve the same conditions for the anion exchange throughout the overall volume of the composite.

First, in our experiments, we tested the behavior of the NCs-in-P(MMA-*co*-LMA) composites without additional treatment. For this, the obtained films containing either only $CsPbBr_3$ NCs or NCs with various amounts of IDD were placed in closed vials and stored at RT in the dark for 30 d. After this period, we detected changes in the color of polymer composites depending on the amount of added IDD (Figure 2c). The changes in the

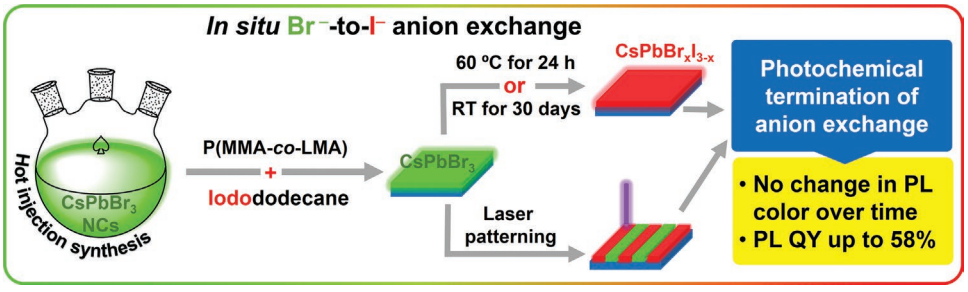

Figure 1. Schematic illustration of the preparation of red- and green-emitting perovskite NCs-in-polymer composites, including in situ anion exchange in polymer films.

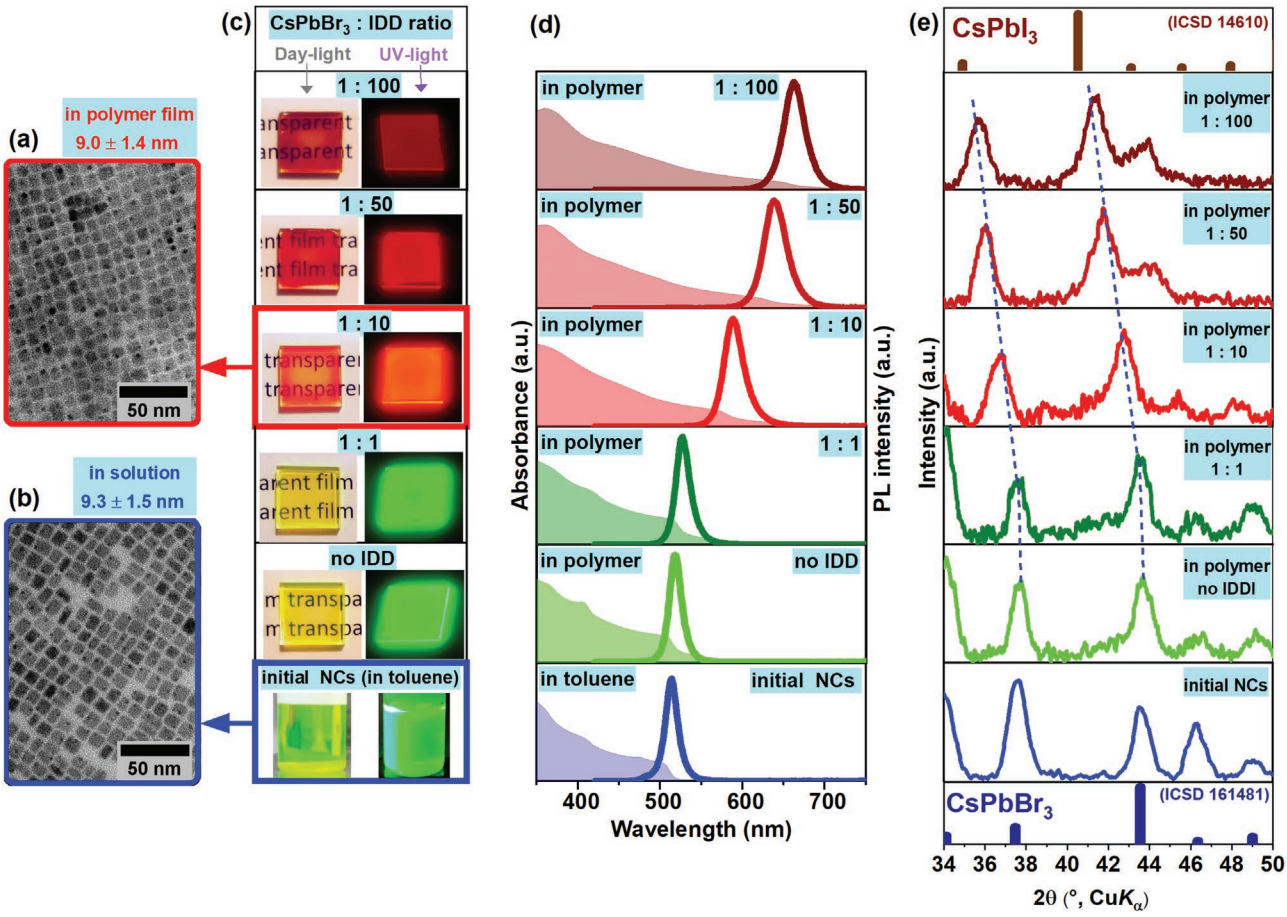

Figure 2. TEM images of a) partially exchanged $CsPbBr_xI_{3-x}$ NCs and b) as-synthesized $CsPbBr_3$ NCs showing shape and size preservation after the anion exchange. c) Photographs, d) absorption and PL spectra, and e) XRD patterns of as-synthesized $CsPbBr_3$ NCs (bottom frame) and of polymer composite films with different molar ratios between embedded $CsPbBr_3$ and IDD after 30 d of storage at RT. The photographs were taken under daylight (left) and UV (366 nm) illumination (right).

optical properties of polymer composites and crystalline structure of NCs embedded in polymer films were monitored by optical spectroscopy and X-ray diffraction (XRD) analysis, correspondingly.

In Figure 2d the absorption and PL spectra of the NCs-in-polymer composites without and with various amounts of added IDD are presented. One can see that there are no significant changes in optical properties of $CsPbBr_3$ NCs after their incorporation into the P(MMA-*co*-LMA) matrix without IDD even after 30 d of storage at RT. The negligible PL redshift (3 nm) may either be caused by a change in the refractive index of the medium or by the self-absorption effect. In contrast, in films containing IDD, significant redshifts in PL and absorption are visible, the value of which correlates with the amount of the iodine precursor added. As shown in Figure 2d, the PL redshift can be tuned from 10 nm in the case of an equimolar amount of IDD to 144 nm upon loading a 100-fold molar excess of the iodine precursor, reflecting the formation of $CsPbBr_xI_{3-x}$ NCs with different iodine-to-bromine ratios.

The morphology of red-emitting $CsPbBr_xI_{3-x}$ NCs obtained through anion exchange directly in the composite using a tenfold molar excess of IDD was exemplarily analyzed via transmission electron microscopy (TEM). For that, the resulting composite was dissolved in dry toluene and dropped onto Formvar-carbon-coated copper grids. As clearly seen in Figure 2a,b, the $CsPbBr_xI_{3-x}$ NCs obtained in the composite preserved the shape and size of the initial $CsPbBr_3$ NCs. The formation of $CsPbBr_xI_{3-x}$ NCs directly in polymer films was also confirmed by XRD-analysis. XRD patterns of as-synthesized $CsPbBr_3$ NCs and the patterns recorded directly from the composites with various $CsPbBr_3$:IDD ratios after storing them for 30 d are displayed in Figure 2e (selected range) and Figure S2 (full patterns, Supporting Information). As follows from the results, the as-synthesized $CsPbBr_3$ NCs have a cubic perovskite structure (ICSD Card No. 14610), with no additional impurity diffraction peaks. The analysis evidences that the incorporation of the NCs into the polymer caused no changes in their crystal structure. At the same time, in the composites with added IDD, the shift of the peaks to smaller angles is observed, where the shift value increases with the increase of the IDD amount. This shift is related to increasing iodine content in forming $CsPbBr_xI_{3-x}$ NCs and is the result of expanding the lattice unit cell due to the incorporation of iodine, possessing a larger radius than bromine.

Thus, the changes observed in the optical properties and structure of the perovskite NCs prove a successful anion

exchange that occurs already at RT without additional treatment. This is a result of the interaction of IDD decomposition products with $CsPbBr_3$ NCs. We assume that the decomposition of IDD in a polymer matrix with the formation of reactive iodine species may occur in various ways. First, IDD can undergo a β-elimination when C_β–H and C_α–I bonds break forming a new C_β=C_α double bond. This process can occur through unimolecular reaction (E1 mechanism), including C_α–X bond dissociation and rapid decomposition of the formed carbenium ion to alkene and proton (Figure S3a, Supporting Information).[40] Second, the composite can contain various Lewis bases, such as water absorbed from the air and traces of amine from the reaction system, which can induce the elimination through a bimolecular reaction (E2 mechanism). In this case, the base eliminates a proton from C_β atom followed by breaking C_β–H bond, forming C_β=C_α double bond, and eliminating I^- (Figure S3b, Supporting Information).[41] Both these processes would lead to the formation of HI in the polymer film, which can diffuse to the surface of embedded $CsPbBr_3$ NCs and engage in the anion exchange reaction. In addition to elimination reactions, decomposition of IDD can occur by a radical mechanism, in which the C–I bond is homolytically cleaved with formation of iodine radicals.

We found that upon a longer storage or upon an additional heat treatment the PL maximum can be shifted even further to the red. **Figure 3** shows a comparative analysis of changes in the optical properties of the composites containing IDD in different ratios after storing them in the dark at RT for 30 and 60 d (corresponding spectra are shown in Figure S4, Supporting Information). The samples were untreated or heated at 60 °C for 24 h before storage. As shown in Figure 3a, the PL redshift in all samples increases with the IDD amounts in the composites, where the untreated samples demonstrate an additional PL redshift after 60 d of storage as compared to the samples stored for 30 d. As expected, we observed a significant redshift after 24 h of the heat treatment, since an increase in temperature accelerates the decomposition reactions of IDD, the diffusion of active species, and the rate of anion exchange. Interestingly, the redshifts in samples of all compositions are the same after storage at RT for 60 d and after 24 h heating at 60 °C, which corresponds to the same degree of the anion exchange process. Samples with a 100-fold excess of IDD heated to 60 °C for 24 h showed a PL maximum at 677 nm, which then shifted to 682 nm after subsequent storage for 60 d. Considering that the same redshift (up to 682 nm) is observed, we may conclude that a complete anionic substitution occurred with the formation of $CsPbI_3$ NCs under these conditions. A very similar PL maximum position was observed after the complete Br^--to-I^- anion exchange in $CsPbBr_3$ NCs conducted in a solution (690 nm)[15] and in $CsPbI_3$ NCs obtained in a direct synthesis (691 nm,[10] 690 nm[5]). Thus, we can assert the possibility of the complete anion exchange in $CsPbBr_3$ NCs embedded in a solid polymer matrix.

As shown in Figure 3b, full width at half maximum (FWHM) values for all samples were within 75–112 meV. The general trend is a slight broadening of the PL bands for composites with $CsPbBr_3$:IDD ratios of 1:1, 1:10, and 1:50, which indicates the formation of the mixed alloy composition of $CsPbBr_xI_{3-x}$. At the same time, narrowing of the bands in the case of

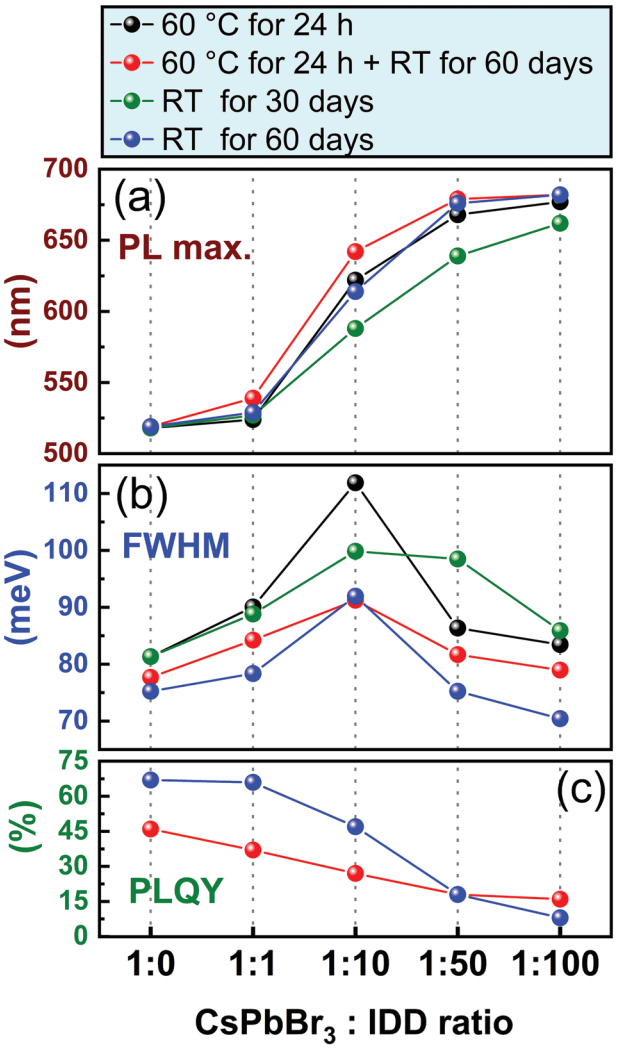

Figure 3. Change of a) PL maximum, b) PL spectral width, and c) PLQY of NCs-in-polymer composites with the various ratios between embedded $CsPbBr_3$ NCs and IDD, and upon the treatment under various conditions summarized in the top panel.

1:100 ratio can be considered as an additional confirmation of the complete exchange yielding $CsPbI_3$ NCs. In addition, there is a narrowing of the PL bands for both heated and RT samples after long-term storage implying the homogenization of the NC composition over time. As one can see in Figure 3c, the PLQY of the composites drops after 60 d of storage for both heated (46%) and RT samples (67%), even in the case of composites without IDD, as compared to the PLQY of the initial NCs in toluene (90%). This drop can be explained by the low stability of cesium lead halide NCs against moisture and oxygen from the air and insufficient protective properties of the P(MMA-*co*-LMA) matrix. Further, a more significant drop in PLQY in the heated samples may be associated with partial depolymerization of P(MMA-*co*-LMA) accompanied by the formation of free radicals damaging embedded NCs. The PLQY monotonically decreases with the redshifts for all samples. The same trend was previously observed in the Br^--to-I^- anion exchange in $CsPbBr_3$ performed in colloidal solutions.[16]

As lead halide-based perovskites are known for their high intrinsic anion mobility, the rate and completeness of the anion exchange depend mainly on the reactivity and the concentration of the precursor. In the samples studied in this work, anion exchange in a solid polymer matrix is limited by the IDD decomposition rate and the diffusion rate of the reactive species to the NC surface. To overcome these limitations, we used an up to 100-fold excess of IDD relative to the amount of $CsPbBr_3$ in the composite. Such a high concentration of the iodine source in the polymer film significantly accelerates the anion exchange. Still, an unreacted precursor in the composite can lead to further changes of optical properties, especially at long-time operation. To make the process more controllable, we here propose a simple but efficient method for terminating the anion exchange in the composite. This termination can be applied to fix the desired PL color despite of the excess of the iodine precursor still available in the film.

Exploring different ways of treatment of our composites, we found that irradiation of the as-prepared sample with ratio $CsPbBr_3$:IDD = 1:10 by a 366 nm UV-light during 24 h did not affect its PL color. Further, we found that after such treatment the sample lost its ability to undergo the anion exchange reaction. Neither during the storage for 30 d at RT nor after heating at 60 °C for 24 h were any changes detected in the PL for these UV-treated samples. We also found that a similar effect can be achieved even quicker, e.g., in 3 h if the 366 nm UV-light treatment was carried out under vacuum (3×10^{-2} mbar), as shown in Figure S5 (Supporting Information).

To disentangle the effect of the UV-light/vacuum treatment, four identical NCs-in-polymer composites with $CsPbBr_3$:IDD = 1:10 were prepared. Three of them were exposed to the UV-light/vacuum for 0.5, 2, and 3 h, and then heated at 60 °C for 24 h (samples *0.5UV/H*, *2UV/H*, and *3UV/H*, respectively, in **Figure 4**a). The fourth was first heated at 60 °C for 24 h and then was exposed to the UV-light for 3 h (sample *H/3UV*). As the result, the samples treated with UV-light showed a significantly smaller PL redshift after the heating stage (Figure 4b) than the same composite not irradiated with UV-light (Figure 3a). Thus, after the UV-light treatment for 0.5, 2, and 3 h, the optical redshift after heating was 55, 30, and 17 nm, respectively, while heating the nonirradiated composite resulted in a redshift of 96 nm. At the same time, sample *H/3UV* showed almost identical optical properties (PL_{max} = 615 nm) to the sample obtained in the previous experiment (PL_{max} = 622 nm) under the same conditions but without UV-light irradiation. It is worth noting that the PLQY of perovskite NCs in sample *H/3UV* (57%) is commensurate with the PLQY of $CsPbI_3$ NCs (58%) obtained in solution by the same method as the original green emitting $CsPbBr_3$ NCs used to prepare the composites.[10]

We further observed that the samples obtained after irradiation with the UV-light demonstrated no considerable changes in optical properties after 30 d of further storage (Figure 4c,d), unlike the composites discussed above (compare with Figures 2 and 3). We assume that under exposure to 366 nm UV-light, IDD can decompose at a significantly higher rate than the rate of the anion exchange at RT. This process can be considerably accelerated under vacuum. It is important to note that the termination is also possible, if the sample is subjected to vacuum in absence of UV-light (room light only). In this case,

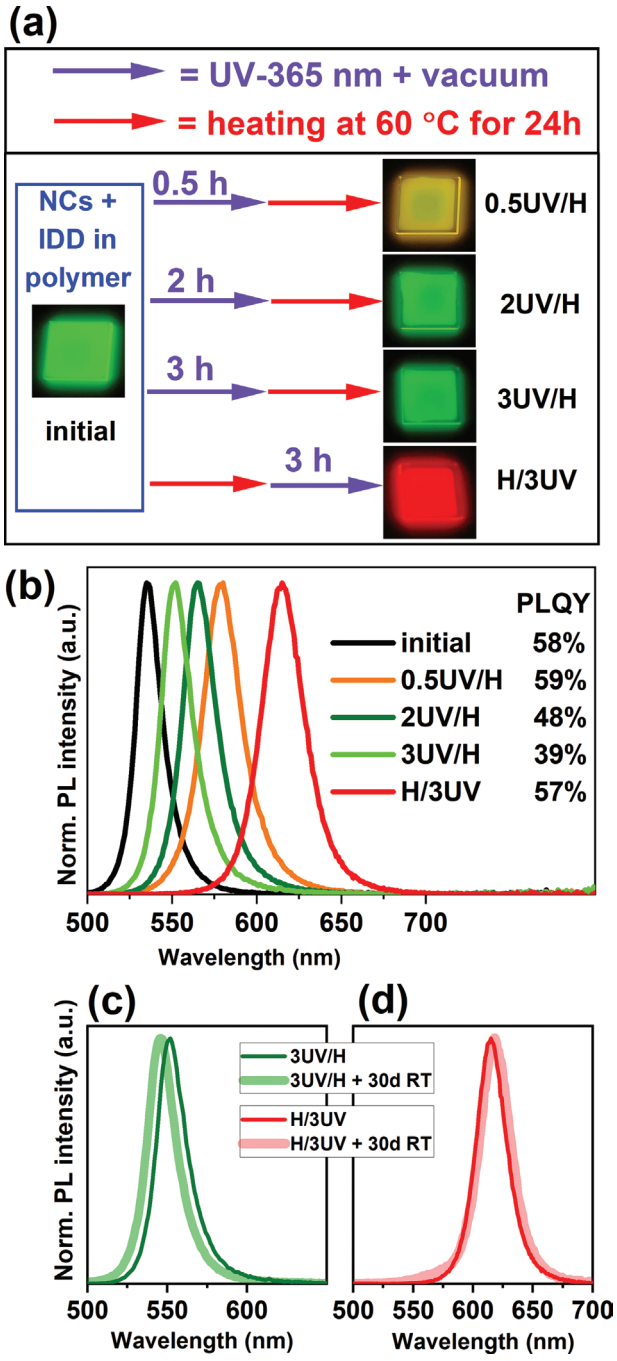

Figure 4. a) Schematic illustration of the experiments on removing IDD from NCs-in-polymer composites under vacuum and UV irradiation and photographs of the corresponding films taken under 366 nm illumination. b) PL spectra and PLQY values of the composite films after the UV/vacuum treatment; c,d) comparison of PL spectra of the films after the UV/vacuum treatment and after further storage at RT for 30 d.

however, the complete deactivation of IDD takes at least three times longer, which can be considered as technologically less attractive.

As IDD has an intense absorption line at 257 nm and the polymer is transparent for light in the UV–vis range starting from 250 nm, the IDD removal process can be monitored

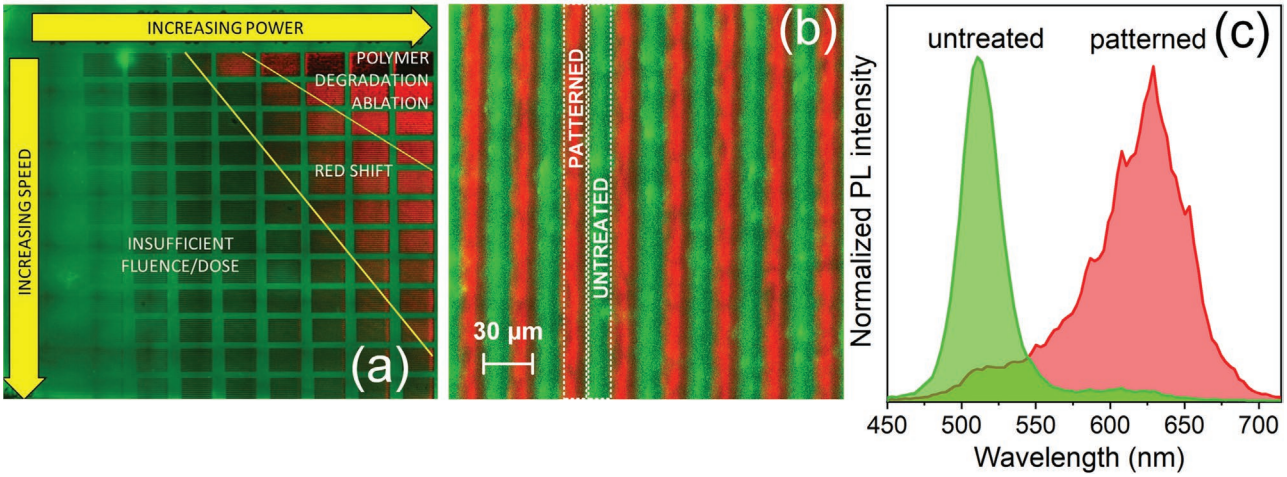

Figure 5. a) Example of operating windows with different color-shifting effectiveness in laser patterning. b) High-resolution $xy\lambda$ imaging of a patterned area showing line tracks with a resolution of 15 µm. c) Micro-PL spectra of the untreated and patterned zones belonging to the two regions of interest shown in (b).

using UV–vis absorption spectroscopy. For this purpose, polymer composites containing IDD with or without $CsPbBr_3$ NCs were deposited on quartz substrates and irradiated with a 366 nm UV light under both vacuum and ambient conditions. Absorption spectra were recorded at different time intervals to monitor changes in the samples (Figure S6a,b, Supporting Information). As shown in Figure S6a,b, there is a significant decrease in the optical density in the area of IDD absorption indicating its removal from the composite under the UV treatment. In addition, we achieved approximately the same level of IDD removal if the samples were irradiated either for 3 h under vacuum or for 24 h under ambient conditions. The same behavior is observed in the case of composites containing only IDD without NCs.

As neither the matrix nor IDD absorbs light at 366 nm and the precursor removal occurs even without $CsPbBr_3$ NCs, we assume the following mechanism for the observed effect. As it is known, iodoalkanes are unstable compounds due to the presence of a weak C—I bond and decompose during storage with the formation of various iodine species (such as IO_3^-, I_2, I_3^-, etc.). These species can contribute to the weak absorption of UV light between 300 and 450 nm observable in Figure S6 (Supporting Information). For example, triiodide (I_3^-) has high absorption at the wavelengths of 293 and 364 nm.[42] Being photoactivated, these species participate in the formation of volatile products easily escaping from the matrix. This process is evidently accelerated under vacuum. The fast removal of the IDD decomposition products shifts the equilibrium of this process toward further decomposition.

At this point, we can conclude that our transparent and processable composite material possesses narrow PL with high QY in the green spectral region, which can be precisely tuned to the red spectral region. This tuning can be controllably accelerated by increasing the concentration of the iodine precursor or by elevating the temperature; moreover, the color of emission can be fixed, if the tuning is terminated by the proper UV/vacuum treatment. The properties mentioned above fit perfectly the requirements for laser patterning, which is designed to induce local chemical transformation of appropriate precursors directly in a transparent matrix.

The pattering was performed using a 355 nm laser having about 1.2 W full power with a repetition rate of 100 kHz. The scheme of the laser setup is shown in Figure S7 (Supporting Information). Samples for patterning were also prepared by drop-casting NCs and P(MMA-*co*-LMA) solutions on glass substrates depicted in Figure S7. An example of a map scanned by the laser is presented in **Figure 5**a, where different combinations of power modulation and scanning speed define three different operating conditions for each pulse repetition rate. Changing the parameters of scanning we found that at low power/pulse energy and/or high scanning speed the cumulated dose was not sufficient enough to induce color shift, but could suffice to deactivate the anion exchange of the green-emitting NCs. At the same time, at high energy per pulse and/or low scanning speed the cumulated dose degraded the polymer matrix and ablated it exposing the glass substrate. Whereas in between these two extreme conditions, a proper color switching from green to red was achieved.

A high-magnification image of a patterned area is presented in Figure 5b demonstrating the possibility to selectively generate 15 µm red-emitting lines interleaved with untreated green-emitting stripes with corresponding PL spectra shown in Figure 5c. These patterned lines were obtained under 150 mW with a pulse repetition rate of 400 kHz and a scanning speed of 30 mm s^{-1} corresponding to a dose slightly above 60 J cm^{-2} and an interaction time of 330 µs.

3. Conclusions

We developed a method to modify the optical properties and composition of cesium lead halide perovskite NCs via anion exchange directly inside polymer films. The use of green-emitting $CsPbBr_3$ NCs obtained by hot-injection approach as templates allows for the formation of yellow- and red-emitting $CsPbBr_xI_{3-x}$ NCs of various compositions through the

controllable reaction with an iodine source. The change in perovskite composition was confirmed by XRD analysis of NCs-in-polymer composites. The obtained composites demonstrate narrow PL in the range of 520–680 nm with PLQY of up to 59%. To adapt the approach for practical applications, we developed a simple yet very efficient method for terminating the anion exchange in the composites after achieving the desired emission color. We also demonstrated that obtained NCs-in-polymer composites are promising materials for laser patterning technology. Using pulsed UV-laser irradiation, we selectively generated red-emitting patterns in the green-emitting film. The application of UV ultrashort laser reduces the energy diffusion inside the thin film matrix guaranteeing a resolution satisfying the needs of many display applications. Laser patterning offers a high flexibility in size and dimensions of patterns. The method could be highly competitive with lithographic processes, especially in the case of small batch production.

4. Experimental Section

Chemicals: Lead acetate trihydrate [$Pb(CH_3COO)_2{\cdot}3H_2O$, 99.999%], cesium carbonate (Cs_2CO_3, 98%), 1-octadecene (ODE, technical grade, 90%), oleic acid (OlAc, 90%), toluene (anhydrous, 99.8%), methanol (99.9%), methyl methacrylate (MMA, 99%, stabilized with ≤30 ppm MEHQ), lauryl methacrylate (LMA, 96%, stabilized with 500 ppm MEHQ), and azobisisobutyronitrile (AIBN, 98%) were purchased from Sigma-Aldrich. Oleylamine (OlAm, ≥ 98%), benzoyl bromide (C_6H_5COBr, 97%), and 1-iodododecane (IDD, 98%, stabilized with 500 ppm Cu) were purchased from Acros Organics. Methanol (≥99.9%) was purchased from Fisher Chemical. MMA and LMA were distilled right before using. AIBN was recrystallized from ethanol. All other chemicals were used as received.

Synthesis of $CsPbBr_3$ NCs: $CsPbBr_3$ NCs were synthesized according to a procedure by Imran et al.[10] with slight modifications using a standard Schlenk line technique. Briefly, 16 mg of Cs_2CO_3 (0.049 mmol), 76 mg of $Pb(CH_3COO)_2{\cdot}3H_2O$ (0.2 mmol), 0.3 mL of OlAc, 1 mL of OlAm, and 5 mL of ODE were degassed under vacuum for 1 h at 100 °C in a 25 mL three-neck round bottom flask and then heated up to 180 °C under Ar flow. Then, the heating mantle was removed, and when the temperature of the solution decreased to 170 °C, 70 µL of benzoyl bromide (0.59 mmol) were rapidly injected. The reaction was quenched immediately after the injection by cooling the flask with an ice-water bath. The crude NC solution was diluted with 5 mL of anhydrous toluene and the resulting mixture was centrifuged at 4000 rpm for 10 min, then at 7000 rpm for 5 min. The supernatant was discarded, and the precipitate was redispersed in 2 mL of dry toluene and kept undisturbed for 24 h in a 4 mL glass vial. Afterward, the clear green supernatant solution was separated from the yellowish precipitate and the obtained stock solution was used for further experiments. The concentration of $CsPbBr_3$ in this solution was estimated using the intrinsic absorption coefficient reported in ref. [43] (see more details in the Supporting Information), and determined to be 7.95×10^{-3} mol L^{-1}.

Synthesis of Poly(methyl methacrylate-co-lauryl methacrylate): The random copolymer P(MMA-*co*-LMA) was synthesized by radical copolymerization of freshly distilled MMA and LMA with a molar ratio of 3:1. Briefly, 143 mg of AIBN (0.869 mmol), 3 mL of MMA (28.17 mmol), and 2.75 mL of LMA (9.39 mmol) were mixed under an inert atmosphere and polymerized at 60 °C for 24 h. The product was precipitated twice from toluene by adding methanol and dried under vacuum at 40 °C/0.01 bar to a constant mass.

Film Preparation: $CsPbBr_3$ NCs exploited for composites preparation were synthesized no more than one week before the use. The composite films were prepared by drop-casting onto warm substrates. For typical film preparation, 80.8 µL of the stock solution of $CsPbBr_3$ NCs in toluene (6.42×10^{-7} mol) and 256.4 µL of pure toluene or toluene solution containing various amounts of IDD (6.42×10^{-7}–6.42×10^{-5} mol, depending on the final composition of the film) were added into a 1.5 mL microcentrifuge tube. The mixture was shaken for 15 min. Then, 97.8 mg of a 23.7% wt solution of P(MMA-co-LMA) in toluene was added into the tube and mixture was shaken for 15 min again. Then, 60 µL of the prepared solution was cast onto a glass substrate of the size of 1×1 cm^2 heated to 70 °C on a hot plate, covering the entire area. After 1 min, the substrate was removed from the heating plate and placed in a closed vial. To prepare thinner films for laser patterning, 60 µL of the solution was drop-cast onto a 1×1 cm^2 glass substrate and spread over the entire area. Then, 54 µL of the solution was imminently removed using a micropipette, leaving a thin solution layer on the substrate. The substrate was then carefully placed onto a heating plate (70 °C) for 1 min to evaporate the solvent.

Anion Exchange: Different reaction conditions of the Br^--to-I^- anion exchange in $CsPbBr_3$ NCs embedded in a P(MMA-*co*-LMA) matrix were investigated. The first two sets of samples (with various amounts of added IDD) were placed in closed vials under air and stored in darkness at RT for 30 and 60 d. The second two sets were heated in an Ar atmosphere at 60 °C for 24 h and then were stored at RT for 30 and 60 d under the same conditions as the first series.

Removing IDD from Polymer Composites: To remove IDD from composite films, they were placed in a quartz tube under vacuum and exposed to a 366 nm UV-lamp (4 W, NU-4 KL from Benda) for 0.5–3 h, as schematized in Figure S5 (Supporting Information). After exposure, the samples were placed in vials that were flooded with argon and heated at 60 °C for 24 h.

Characterization: Absorption spectra were acquired with a Cary 60 spectrophotometer (Varian). PL spectra were recorded on a Fluoromax-4 (Horiba Jobin Yvon, Inc.) spectrofluorometer. Absolute PLQYs were determined by using a Fluorolog-3 spectrofluorometer equipped with a Quanta-ϕ integrating sphere (Horiba Jobin Yvon, Inc.). Transmission electron microscopy was performed on a JEOL JEM-1400 Plus microscope operated at 120 kV. Powder X-ray diffraction patterns were acquired using a Bruker D2 Phaser. The $CsPbBr_3$ NCs dispersed in toluene were drop-cast on a Si wafer. The composite films were delaminated from the substrates and placed on a Si wafer.

Laser Patterning: The films with the thickness of ≈8 µm for patterning were prepared by drop-casting mixtures of $CsPbBr_3$ NCs and P(MMA-*co*-LMA) in toluene on glass substrates as described above. The substrates were then fixed over a glass slider to simplify manipulation during laser patterning and during characterization with confocal microscopy (Figure S7, Supporting Information). The samples were irradiated with an EKSPLA IR5-GR2-UV1 Atlantic series laser by using the third harmonic beamline operating at 355 nm. This beamline can generate about 1.2 W full power with a repetition rate of 100 kHz. The laser emits pulses with a duration of 10 ps, the collimated beam is expanded to a $1/e^2$ diameter of 14 mm and directed collinear to a Z moving stage. The laser beam is then deflected on the samples by a 20 bits Raylase Superscan V digital scanning head and focused with a 100 mm focal F-theta lens. Considering the beam quality $M^2 = 1.3$ and the specifications of the other optical components a $1/e^2$ focal diameter of 10 µm is estimated by calculations and experimentally verified prior tests.

To determine the most appropriate operating conditions, three parameters were modulated: the frequency which in turn is correlated to energy per pulse, the power modulation, and the scanning speed. These three parameters induce different irradiation conditions in terms of pulse fluence, dose (multipulse fluence), and interaction time (for details see the Supporting Information, Figures S7–S9). For each parameter a combination of rectangular zones 0.8×0.5 mm were linearly patterned with a scan step of 40 µm (see Figure S8, Supporting Information). The investigated parameters are summarized in Table S1 (Supporting Information).

Power modulation and repetition rate conditions were mapped in terms of power and energy per pulse delivered on the material by measuring just above the sample surface with a thermopile detector Gentec XLP12-3S-H2-D0. This permitted the authors to count dispersions along the optical path and to evaluate results in terms of energetic parameters on the material. The patterned samples were characterized by a Leica DMi8 confocal microscope equipped with a four-channel Leica TCS SP8 scanning head using a 405 nm diode laser to excite the PL. Spatial emission maps were generated by acquiring, during the scan, the three channels of 430–480, 490–560, and 620–700 nm, while $xy\lambda$ spatial/spectral emission was captured using the highest spectral resolution of 5 nm.

Supporting Information

Supporting Information is available from the Wiley Online Library or from the author.

Acknowledgements

C.M. and A.P. contributed equally to this work. This work was supported by European Union Horizon 2020 research and innovation programme under Grant Agreement 779373, project MILEDI (MIcro quantum dot Light Emitting diode and organic LEDs DIrect patterning). The authors are grateful to Dr. N. Weiß and S. Goldberg for TEM imaging. N.G. appreciates numerous discussions and insights into the photophysics of the quantum dot assemblies from his collaborator and friend Jochen Feldmann, LMU Munich.

Open access funding enabled and organized by Projekt DEAL.

Conflict of Interest

The authors declare no conflict of interest.

Data Availability Statement

The data that support the findings of this study are available from the corresponding author upon reasonable request.

Keywords

anion exchange, cesium lead halide perovskite nanocrystals, direct laser patterning, nanocrystals-in-polymer composites, tunable photoluminescence

Received: January 27, 2022
Revised: March 21, 2022
Published online:

[1] H. Lee, J. Park, S. Kim, S. Lee, Y. Kim, T. Lee, *Adv. Mater. Technol.* **2020**, *5*, 2000091.
[2] F. Zhang, J. Song, B. Han, T. Fang, J. Li, H. Zeng, *Small Methods* **2018**, *2*, 1700382.
[3] J. Lin, Y. Lu, X. Li, F. Huang, C. Yang, M. Liu, N. Jiang, D. Chen, *ACS Energy Lett.* **2021**, *6*, 519.
[4] J. Kang, L.-W. Wang, *J. Phys. Chem. Lett.* **2017**, *8*, 489.
[5] F. Liu, Y. Zhang, C. Ding, S. Kobayashi, T. Izuishi, N. Nakazawa, T. Toyoda, T. Ohta, S. Hayase, T. Minemoto, K. Yoshino, S. Dai, Q. Shen, *ACS Nano* **2017**, *11*, 10373.
[6] A. Dey, J. Ye, A. De, E. Debroye, S. K. Ha, E. Bladt, A. S. Kshirsagar, Z. Wang, J. Yin, Y. Wang, L. N. Quan, F. Yan, M. Gao, X. Li, J. Shamsi, T. Debnath, M. Cao, M. A. Scheel, S. Kumar, J. A. Steele, M. Gerhard, L. Chouhan, K. Xu, X.-G. Wu, Y. Li, Y. Zhang, A. Dutta, C. Han, I. Vincon, A. L. Rogach, et al., *ACS Nano* **2021**, *15*, 10775.
[7] Y. Tong, E. Bladt, M. F. Aygüler, A. Manzi, K. Z. Milowska, V. A. Hintermayr, P. Docampo, S. Bals, A. S. Urban, L. Polavarapu, J. Feldmann, *Angew. Chem., Int. Ed.* **2016**, *55*, 13887.
[8] L. Protesescu, S. Yakunin, M. I. Bodnarchuk, F. Krieg, R. Caputo, C. H. Hendon, R. X. Yang, A. Walsh, M. V. Kovalenko, *Nano Lett.* **2015**, *15*, 3692.
[9] J. Shamsi, A. S. Urban, M. Imran, L. De Trizio, L. Manna, *Chem. Rev.* **2019**, *119*, 3296.
[10] M. Imran, V. Caligiuri, M. Wang, L. Goldoni, M. Prato, R. Krahne, L. De Trizio, L. Manna, *J. Am. Chem. Soc.* **2018**, *140*, 2656.
[11] Y. Dong, T. Qiao, D. Kim, D. Parobek, D. Rossi, D. H. Son, *Nano Lett.* **2018**, *18*, 3716.
[12] X. Li, Y. Wu, S. Zhang, B. Cai, Y. Gu, J. Song, H. Zeng, *Adv. Funct. Mater.* **2016**, *26*, 2435.
[13] Q. Zhong, M. Cao, Y. Xu, P. Li, Y. Zhang, H. Hu, D. Yang, Y. Xu, L. Wang, Y. Li, X. Zhang, Q. Zhang, *Nano Lett.* **2019**, *19*, 4151.
[14] H. Jiang, S. Cui, Y. Chen, H. Zhong, *Nano Sel.* **2021**, *2*, 2040.
[15] G. Nedelcu, L. Protesescu, S. Yakunin, M. I. Bodnarchuk, M. J. Grotevent, M. V. Kovalenko, *Nano Lett.* **2015**, *15*, 5635.
[16] Q. A. Akkerman, V. D'Innocenzo, S. Accornero, A. Scarpellini, A. Petrozza, M. Prato, L. Manna, *J. Am. Chem. Soc.* **2015**, *137*, 10276.
[17] Q. A. Akkerman, G. Rainò, M. V. Kovalenko, L. Manna, *Nat. Mater.* **2018**, *17*, 394.
[18] C. Eames, J. M. Frost, P. R. F. Barnes, B. C. O'Regan, A. Walsh, M. S. Islam, *Nat. Commun.* **2015**, *6*, 7497.
[19] W. Lv, X. Tang, L. Li, L. Xu, M. Li, R. Chen, W. Huang, *J. Phys. Chem. C* **2019**, *123*, 24313.
[20] Y. Wei, Z. Cheng, J. Lin, *Chem. Soc. Rev.* **2019**, *48*, 310.
[21] H. Wang, N. Sui, X. Bai, Y. Zhang, Q. Rice, F. J. Seo, Q. Zhang, V. L. Colvin, W. W. Yu, *J. Phys. Chem. Lett.* **2018**, *9*, 4166.
[22] R. K. Gautam, S. Das, A. Samanta, *J. Phys. Chem. C* **2021**, *125*, 24170.
[23] F. Krieg, S. T. Ochsenbein, S. Yakunin, S. ten Brinck, P. Aellen, A. Süess, B. Clerc, D. Guggisberg, O. Nazarenko, Y. Shynkarenko, S. Kumar, C.-J. Shih, I. Infante, M. V. Kovalenko, *ACS Energy Lett.* **2018**, *3*, 641.
[24] Q. A. Akkerman, D. Meggiolaro, Z. Dang, F. De Angelis, L. Manna, *ACS Energy Lett.* **2017**, *2*, 2183.
[25] Z. Chen, B. Zhou, J. Yuan, N. Tang, L. Lian, L. Qin, L. Zhu, J. Zhang, R. Chen, J. Zang, *J. Phys. Chem. Lett.* **2021**, *12*, 3038.
[26] C. Guhrenz, A. Benad, C. Ziegler, D. Haubold, N. Gaponik, A. Eychmüller, *Chem. Mater.* **2016**, *28*, 9033.
[27] F. Zhang, Z.-F. Shi, Z.-Z. Ma, Y. Li, S. Li, D. Wu, T.-T. Xu, X.-J. Li, C.-X. Shan, G.-T. Du, *Nanoscale* **2018**, *10*, 20131.
[28] I. Konidakis, K. Brintakis, A. Kostopoulou, I. Demeridou, P. Kavatzikidou, E. Stratakis, *Nanoscale* **2020**, *12*, 13697.
[29] I. Konidakis, A. Karagiannaki, E. Stratakis, *Nanoscale* **2022**, *14*, 2966.
[30] J.-Y. Sun, F. T. Rabouw, X.-F. Yang, X.-Y. Huang, X.-P. Jing, S. Ye, Q.-Y. Zhang, *Adv. Funct. Mater.* **2017**, *27*, 1704371.
[31] S. Liang, M. Zhang, G. M. Biesold, W. Choi, Y. He, Z. Li, D. Shen, Z. Lin, *Adv. Mater.* **2021**, 2005888.
[32] Y. Wei, X. Deng, Z. Xie, X. Cai, S. Liang, P. Ma, Z. Hou, Z. Cheng, J. Lin, *Adv. Funct. Mater.* **2017**, *27*, 1703535.
[33] Y. Li, Y. Lv, Z. Guo, L. Dong, J. Zheng, C. Chai, N. Chen, Y. Lu, C. Chen, *ACS Appl. Mater. Interfaces* **2018**, *10*, 15888.
[34] F. Boussoufi, M. Pousthomis, A. Kuntzmann, M. D'Amico, G. Patriarche, B. Dubertret, *ACS Appl. Nano Mater.* **2021**, *4*, 7502.

[35] S. N. Raja, Y. Bekenstein, M. A. Koc, S. Fischer, D. Zhang, L. Lin, R. O. Ritchie, P. Yang, A. P. Alivisatos, *ACS Appl. Mater. Interfaces* **2016**, *8*, 35523.
[36] H. Kim, N. Hight-Huf, J. Kang, P. Bisnoff, S. Sundararajan, T. Thompson, M. Barnes, R. C. Hayward, T. Emrick, *Angew. Chem., Int. Ed.* **2020**, *59*, 10802.
[37] Q. Zhou, Z. Bai, W. Lu, Y. Wang, B. Zou, H. Zhong, *Adv. Mater.* **2016**, *28*, 9163.
[38] J. S. Manser, J. A. Christians, P. V. Kamat, *Chem. Rev.* **2016**, *116*, 12956.
[39] F. Antolini, L. Orazi, *Front. Chem.* **2019**, *7*, 252.
[40] *Addition and Elimination Reactions of Aliphatic Compounds* (Eds: C. H. Bamford, C. F. H. Tipper), Elsevier Science, New York **1973**.
[41] M. B. Smith, J. March, *March's Advanced Organic Chemistry*, Wiley, Hoboken, NJ **2006**.
[42] M. Tułodziecki, G. M. Leverick, C. V. Amanchukwu, Y. Katayama, D. G. Kwabi, F. Bardé, P. T. Hammond, Y. Shao-Horn, *Energy Environ. Sci.* **2017**, *10*, 1828.
[43] J. Maes, L. Balcaen, E. Drijvers, Q. Zhao, J. De Roo, A. Vantomme, F. Vanhaecke, P. Geiregat, Z. Hens, *J. Phys. Chem. Lett.* **2018**, *9*, 3093.